A local insulin reservoir in Drosophila alpha cell homologs ensures developmental progression under nutrient shortage

Suhrid Ghosh, Weihua Leng, Michaela Wilsch-Bräuninger, Mariana Barrera-Velázquez, Pierre Léopold, Suzanne Eaton

A local insulin reservoir in *Drosophila* alpha cell homologs ensures developmental progression under nutrient shortage

Suhrid Ghosh[1,2*], Weihua Leng[1], Michaela Wilsch-Bräuninger[1], Mariana Barrera-Velázquez[1,3], Pierre Léopold[4*#] and Suzanne Eaton[1,2,5]

[1]Max Planck Institute of Molecular Cell Biology and Genetics, Pfotenhauerstraße 108, 01307 Dresden, Germany

[2]Biotechnologisches Zentrum, Technische Universität Dresden, Tatzberg 47/49, 01307 Dresden, Germany.

[3]Undergraduate Program on Genomic Sciences, Centro de Ciencias Genómicas, UNAM, Cuernavaca, Morelos 62210, Mexico

[4]Institut Curie, PSL Research University, CNRS UMR3215, INSERM U934, 26 Rue d'Ulm, 75005 Paris, France.

[5]Deceased

*Authors for correspondence: ghosh@mpi-cbg.de, pierre.leopold@curie.fr

[#]Lead contact

Twitter handles: Suhrid Ghosh (@ghoshnotgosh), Leopold Lab (@LeopoldLab), Eaton Lab (@eatonlab)

Summary (189 words)

Insulin/IGF signalling (IIS) controls many aspects of development and physiology. In *Drosophila*, a conserved family of insulin-like peptides called Dilps is produced by brain neurosecretory cells and regulates organismal growth and developmental timing. To accomplish these systemic functions, the Dilps are secreted into the general circulation and signal to peripheral tissues in an endocrine fashion. Here, we describe the local uptake and storage of Dilps in the Corpora Cardiaca (CC), an endocrine organ composed of *alpha* cell homologs known to produce the glucagon-like Adipokinetic hormone (AKH). We show that Dilp uptake by the CC relies on the expression of an IGF-binding protein called ImpL2. Following their uptake, immuno-gold staining demonstrates that Dilps are co-packaged with AKH in dense-core vesicles for secretion. In response to nutrient shortage, this specific Dilp reservoir is released and activates IIS in a paracrine manner in the prothoracic gland. This stimulates the production of the steroid hormone ecdysone and initiates entry into pupal development. We therefore uncover a sparing mechanism whereby insulin stores in CC serve to locally activate IIS and the production of ecdysone in the PG, accelerating developmental progression in adverse food conditions.

Keywords

insulin, ecdysone, nutrition, hormone secretion, Drosophila

Introduction

Insulin and insulin-like growth factors (IGFs) are conserved modulators of growth and metabolic homeostasis. They are produced by specific endocrine organs in response to nutrient availability and stimulate peripheral tissues through two main routes. Circulating insulins and IGFs act in an endocrine manner on distant organs through mechanisms of secretion and action that have been extensively studied [1–3]. In several instances, insulin/IGFs are also produced and act locally. This is the case for IGF-I produced in peripheral organs like bone chondrocytes, which acts in an autocrine manner [4]. Local insulin/IGF signalling is also key for the development and homeostasis of the central nervous system, which is separated from the systemic circulation by the blood-brain barrier [5]. In mammalian brains, IGF-I expression is spatially and temporally controlled, participating in the rapid proliferation of neural stem cells (NSCs) [6]. IGF-I is expressed in neurons, astrocytes and NSCs, contributing to both paracrine and autocrine signaling [7].

In the *Drosophila* model, a subset of insulin/IGFs called *Drosophila* insulin-like peptides (Dilps) is expressed in neurosecretory cells and contributes to systemic activation of insulin/IGF signaling (IIS). Similar to mammals, local brain expression of Dilps in glial cells also contributes to coupling NSC proliferation with systemic metabolic status [8,9].

In parallel, local activation of IIS can be triggered by alternative routes, providing the possibility to uncouple insulin/IGF signaling from nutrient availability. The role of this uncoupling is exemplified in the case of "brain sparing" a phenomenon observed in many species, including human, whereby moderate nutrient deprivation affects primarily body growth, while brain growth is preserved [10]. The molecular mechanism of brain sparing has been addressed in *Drosophila*. It is associated with the specific activation of neuroblast growth through local production of the ligand Jelly belly (Jeb) and activation of the Anaplastic lymphoma kinase (Alk) receptor upstream of PI-3-kinase, even in the absence of nutrients [11].

Here, we unravel a distinct mechanism locally uncoupling insulin release from the presence of nutrients and leading to the maintenance of IIS activation in a key endocrine organ during development. The initial observation of a pool of Dilps accumulating in neurosecretory cells called the corpora cardiaca (CC) [12], suggested the possibility that these insulins could activate IIS under specific conditions, in a way distinct from their systemic function. Indeed, the CC cells do not produce insulins, but rather a glucagon-like hormone called AKH, whose release is stimulated by nutrient shortage. Our present work unravels some features of the mechanism of uptake of insulins by the CC. We show that, conversely to systemic insulins, CC insulins are released in response to nutrient deprivation. We further demonstrate that the local release of CC insulins upon starvation maintains high IIS levels in the prothoracic gland (PG), which produces the

steroid ecdysone. Finally, we establish that the local activation of IIS in the PG secures a fast transition to pupal development in absence of nutrients.

Therefore, our work uncovers a distinct mechanism of organ-sparing, whereby a pre-accumulated store of Dilps is released in adverse food conditions and ensures fast developmental progression through steroid production.

Results

Corpora cardiaca cells take up Dilp2 and 5

The Corpora Cardiaca (CC) is part of the ring gland (RG), a composite endocrine organ located in the vicinity of the larval central nervous system (CNS) (Figure 1A). Apart from the CC, two other endocrine tissues - the prothoracic gland (PG), which synthesizes ecdysone, and the corpora allata (CA), which synthesizes the juvenile hormone – together form the RG (Figure 1A). CC cells are neurosecretory in nature and extend processes that terminate in the larval aorta and the PG (Figure 1A). The IPCs, located in the pars intercerebralis of the larval brain, also project to the aorta (Figure 1A). Previous work describes a strong accumulation of anti-Dilp2 immunoreactivity in the corpora cardiaca (CC) [12], in addition to the one observed in the cell bodies of IPCs [13]. However, whether CC cells express the Dilp2 gene has not been investigated.

In order to clarify the presence and production of Dilp2 in CC cells, we co-labelled the IPC projections by over-expressing a GFP-tagged Synaptotagmin-1 (*SYT1-GFP*) using a *dilp2-gal4* driver (*IPC>SYT1-GFP*, Figure 1B) and anti-Dilp2 immunostaining. We confirmed the presence of IPC processes containing DILP2 and innervating the aorta (Figure 1B). Additionally, Dilp2 could also be detected without GFP colocalization in the CC (Figure 1B). Expressing *SYT1-GFP* using a CC-specific GAL4 driver (*akh-gal4*), we confirmed that Dilp2 indeed co-localizes with GFP in CC cells and their processes projecting on the PG and the aorta (Figure 1C). The CC also stain for anti- Dilp5, and both Dilp2 and Dilp5 show high degree of subcellular colocalization, suggesting that these two Dilps may serve a common function in the CC (Figure 1D, anti-HRP antibodies stain neuronal membranes in *Drosophila* [14] and serve to highlight the CC). Presence of Dilp2 and Dilp5 in the soma of the CC cells could either be due to a transient expression in the CC or their uptake by the CC from a pool initially produced by the IPCs. To address this point, we specifically knock-down *DILP2* or *DILP5* expression in the IPCs. This led to their loss in CC cells (Figures 1E-H), indicating that the IPCs are the only source of Dilp production, followed by their specific uptake in the CC. Of note, the knock-down of Dilp5 expression in the IPCs did not affect the Dilp2 signal in the CC (Figure S1), suggesting that these two Dilps are taken up separately in these cells.

ImpL2 mediates the uptake of Dilp2 and Dilp5 in the Corpora cardiaca

In addition to the canonical insulin receptor (dInR), *Drosophila* larvae express another insulin-binding protein called ImpL2. ImpL2 binds circulating Dilp2 and Dilp5, resulting in the downregulation of insulin/IGF- signalling (IIS) in target tissues [15,16]. Beside tumorous imaginal discs and fat body [16,17], which produce a circulating form of ImpL2, a subset of neurons in the larval brain express the *ImpL2* gene [15]. Using specific anti-ImpL2 antibodies, we also detected ImpL2 in the CC (Figure 2A). Similar staining patterns between ImpL2 and Dilp2 suggests that they may be partially bound inside the CC. Staining for ImpL2 in *Dilp2/Dilp5* double knock-out larvae ruled out a possible staining artefact due to cross-reactivity of the respective antibodies (Figure S2A,B). Additionally, our results show that the presence of ImpL2 in the CC is independent of Dilp2 and 5 production (Figure S2A,B).

ImpL2 binds to Dilps but, unlike dInR, does not have a trans-membrane domain [18]. A previous study [19] showed that a membrane-associated form of ImpL2 produced in a few brain neurons binds Dilp2 and facilitates its contact with dInR, resulting in activation of intracellular IIS signalling. While dInR is recycled to the membrane after endocytosis, the ImpL2-Dilp2 complex is then degraded [19]. In order to clarify the mechanism of Dilp uptake by the CC, we knocked-down dInR and ImpL2 and compared the amount of Dilps present in CC cells. dInR and ImpL2 knock-down were first controlled for their efficacies in the wing disc and CC respectively (Figure S2C-D and S2E-F). While silencing *dInR* in CC had no effect on Dilp2 localization, *ImpL2* knock-down significantly reduced Dilp2 staining in the soma of CC cells (Figures 2b and 2c). Similar results were obtained for Dilp5 localisation (Figure S2G). The knock-down of *dInR* reduces CC cell area and shows a slight increase in mean intensities of Dilp2 (Figures 2c) and 5 (Figure S2G). Silencing ImpL2 in CC did not affect expression of ImpL2 in brain neurons (Figures S2F). We conclude from these experiments that CC cells require ImpL2, but not dInR, to take up Dilps. Next, we ensured that preventing Dilp uptake in the CC does not affect endogenous glucagon-like AKH production by staining CC with anti-AKH antibodies (Figures 2d and 2e). Therefore, ImpL2 silencing in CC cells is an efficient tool to study the physiological function of the pool of Dilps present in the CC. Of note, other DILP2-containing projections run from the brain to the Corpora Allata (CA)[20] (Figure S3). However, these are not affected when preventing Dilp uptake in CC cells (Figure S3).

Corpora cardiaca act as a functional Dilp store

Larvae lacking Dilp2 and Dilp5 show reduced growth during larval stages, require extended time to develop and produce smaller adults [21]. To evaluate the contribution of the CC store of Dilp2 and Dilp5 to general IIS, we measured the developmental time, larval growth and adult size of animals devoid of ImpL2 in CC cells, therefore lacking Dilp accumulation in CC. We observed that larvae of the *CC>ImpL2-RNAi*

131 genotype pupariated approx. 10 hr in advance compared to controls (Figure 3A). However, pupal volume
132 (a measure of total larval growth), adult mass and wing area were not modified (Figure 3B-D). This
133 indicates that animals devoid of their CC-Dilp store experience accelerated growth without affecting final
134 size. Measuring larval mass across the L3 stage, we indeed found that removal of CC-Dilps leads to an
135 increase in larval growth rate (Figure 3E). Accelerated growth was previously observed upon a general
136 increase in intracellular IIS [22] or over-expression of *DILP2* [23,24] during larval development. When measuring
137 circulating Dilp2 from *CC>ImpL2-RNAi* larvae, we found it doubling compared to controls (Figure 3F). To
138 support this finding, we also found elevated levels of fat body IIS at 104hr AEL compared to control
139 genotypes, measured as the relative distribution of the transcription factor dFOXO between nucleus and
140 cytoplasm (Figure 3G and 3H). Therefore, preventing Dilp uptake in the CC increases circulating Dilp2
141 levels and accelerates growth.
142
143 CC-Dilps are packaged for co-secretion with the Glucagon homolog AKH
144 Our previous results indicate that approximately equal amounts of Dilp circulate in the hemolymph and
145 are sequestered in the CC cells (Figure 3F). We therefore examined the secretion of this major pool of CC-
146 Dilp. Based on colocalization using light microscopy, it was previously proposed that ImpL2/Dilp2
147 complexes are degraded through the late endosomal route in *ImpL2*-expressing neurons [19]. Given the
148 small size of the soma of CC cells, we used electron microscopy to identify Dilp-containing structures
149 inside the CC cells (Figure 4A). Stitching several high-resolution images from a single tissue section (Figure
150 S4) shows the overall organization of the cytoplasm of a CC cell , i.e. large networks of ER, occasionally
151 interspersed with Golgi complexes, and clusters of dense-core secretory vesicles (DCVs) occupying the
152 perinuclear space (Figure 4B). This architecture is in line with the capacity of CC cells to secrete the
153 glucagon-like hormone AKH, and similar observations have been made in other insects [25]. When probed
154 for Dilp5 using immuno-gold staining, CC cells showed high reactivity in clusters of DCVs compared to the
155 rest of the cytoplasm (Figures 4C and 4D). Probing simultaneously for Dilp2 and 5 using gold particles of
156 two different sizes, we observed a co-localization of both Dilps not only in DCVs, but also in multi-vesicular
157 bodies (MVBs) (Figure 4E). MVBs form in the late endocytic pathway and are responsible for recycling and
158 degradation of endocytic compartments [26,27]. Alternatively, they also give rise to secretory granules [28]. Our
159 results therefore suggest that Dilp2 and 5 are taken up and packaged into secretory DCVs, making the CC
160 cells a potential alternative source of circulating insulin in the larva.
161 CC cells produce the glucagon-like hormone AKH and release it under nutrient-limiting conditions [12].
162 When probing CC cells for AKH and Dilp2 using two differently-sized gold particles, we found that AKH and
163 Dilp2 co-localize in the same DCVs (Figure 4F). We confirmed the two distinct gold particle populations by

plotting the size distribution (Figure 4F). Therefore, two functionally antagonistic hormones, AKH and Insulin, are co-packaged in the same secretory structures, raising the intriguing possibility that they are released by CC cells in the same physiological context (i.e. limiting nutrients).

CC-Dilps control the time to pupariation under limiting nutrients.

What could be the physiological role of the pool of CC-insulin? During the late larval period, holometabolous insects pass through two pre-metamorphosis checkpoints, called critical weight and minimal viable weight, which ensure that energy stores are sufficient before transiting to the non-feeding pupal stage [29]. During *Drosophila* development, these two checkpoints are reached at the same larval weight and therefore collectively referered to as nutrient restriction checkpoint (NRC) [30]. When starved before the NRC, *Drosophila* larvae do not grow and never pupariate. By contrast, early observations indicate that when starved after the NRC, *Drosophila* larvae pupariate significantly earlier than fed controls (Figure 5A,B and S5) [31,32].

Several lines of evidence suggest that the pool of CC-Dilps induces early pupariation upon starvation post-NRC. First, we noticed that, when comparing fed and starved conditions, the acceleration observed for *CC>w1118* controls is absent in the *CC>ImpL2-RNAi* background (Figure 5C). As described before (see Figure 3A,E), fed *CC>ImpL2-RNAi* larvae pupariate earlier than fed *CC>* controls due to increased circulating Dilps and accelerated growth. In *CC>ImpL2-RNAi* larvae, the difference between fed and starved conditions is abrogated (marked as a grey area in Figures 5B,C and S5). We then found that CC-Dilp pool completely disappears upon starvation (Figure 5D,E). Inactivating the CC by expressing Kir2.1 resulted in retention of Dilp2 (Figure 5F,G), thus confirming that starvation stimulates the release of CC insulin, reminiscent of what is observed in case of AKH secretion [33]. The transition into pupal development requires a surge of ecdysone production and previous work indicate that activation of IIS is required for ecdysone biosynthesis by the PG [34,35]. Therefore, our observation that CC cells send projections to the PG raises the possibility of a local delivery of Dilps to the PG in response to starvation. To test this hypothesis, we compared the levels of circulating Dilp2 in *CC>* and *CC>ImpL2-RNAi* larvae under different nutritional conditions. In fed conditions, suppressing the CC-Dilp pool leads to an increase in circulating Dilp2 (Figure 5H). However, during starvation post-NRC, no circulating Dilp2 is detected either in *CC>* or *CC>ImpL2* conditions (Figure 5I), indicating that the release of the CC pool of Dilp2 does not contribute to increasing systemic Dilp2. In parallel, we measured the nucleus/cytoplasm ratio of dFOXO in fat cells as a marker of peripheral IIS (Figure 5J,K). Again, no difference in adipose IIS was observed between *CC>* and *CC>ImpL2-RNAi* larvae starved after the NRC, indicating that under these conditions CC-Dilp2 does not contribute to general IIS. In contrast, we observed that post-NRC starvation induces an increase in nuclear localization

of dFOXO in PG cells of *CC>ImpL2-RNAi* but not of *CC>* control animals (Figure 5L,M). This indicates that CC-Dilps contribute to maintaining a high level of IIS activation in the PG in response to post-NRC starvation. To confirm the role of IIS in the PG on ecdysone production, we checked for ecdysone target gene expression upon starvation (Figure 5N). Starved *CC>* control larvae showed an upregulation of early ecdysone targets like *broad* and *DHR4* [36,37], compared to fed *CC>* controls (Figure 5N). However, *CC>ImpL2-RNAi* larvae did not show any significant change in early ecdysone target genes expression between fed and starved conditions. Notably, late ecdysone target genes like *E74A* and *ftz-f1* [38] showed no change in expression level between conditions and genotypes within this 12-hour time frame. Finally, In line with our finding that starved *CC>* control larvae pupariate earlier under these conditions, we conclude that the pool of CC-Dilps contributes to a local activation of IIS in PG cells, maintaining their capacity to synthesize ecdysone and allowing a premature transition into pupal development in response to late starvation.

Discussion

In this study, we re-evaluate a previous observation whereby glucagon-producing cells take up insulin peptides, and demonstrate the relevance of this phenomenon during *Drosophila* larval development. In the course of early studies on *Drosophila* insulin-producing cells [12], it was indeed noted that larval CC cells strongly label for Dilp2 peptides. This puzzling observation suggested that the larval CC could serve the role of a so-called "neurohemal" organ, storing Dilps for delivery in the general circulation under specific conditions. However, the mechanistic and functional aspects of this Dilp store were unknown. Our study now sheds new light on the role of CC-Dilps, linking them to another unexplained observation, the starvation-induced, premature transition of *Drosophila* larvae into pupal development (Beadle et. al., 1938) .

Accelerating development upon post-critical weight starvation

Drosophila populations can suffer episodes of nutrient limitation, particularly during the larval period when mobility of individuals is limited, preventing them from exploring alternative food sources. When larvae endure full starvation passed the so-called nutrient restriction checkpoint (NRC), an acceleration of pupariation is observed and animals transit faster to an adult reproductive state, with a trade-off on individual size. This contrasts with the observation that Dilp secretion is inhibited by starvation [24], leading to a reduction of circulating hormone levels. Such reduction should indeed affect the production of ecdysone, which relies on IIS in PG cells [34]. Our present work indicates that upon limiting nutrients, CC

cells secrete stored Dilps to the PG in a paracrine fashion (through PG-specific projections) without affecting systemic IIS. The CC-derived Dilps sustain IIS in PG cells, providing the necessary signalling input for ecdysone production and accelerated pupariation. Indeed, IIS activation could prevent starvation-induced autophagy in PG cells, which has been shown to block ecdysone production in condition of a pre-NRC starvation, by shunting cholesterol away from the biosynthetic pathway [39]. Recent evidence suggests that alternative nutrient-independent growth factors such as Jelly-belly (Jeb) can also act on PG cells to stimulate IIS and ecdysone production [40]. Jeb and Dilps could constitute separate inputs on ecdysone production, explaining why removal of CC Dilps only affects acceleration upon nutrient restriction but does not delay pupariation. Whether CC-Dilps are uniquely targeted to the PG, and through which mechanism, are still open questions.

Our observation of a co-packaging of Dilps and AKH in core dense vesicles in CC cells opens the possibility that the two hormones are released concomitantly on PG cells. In line with this, a recent study by Hughson and colleagues [41] identifies AKH-positive CC projections on PG cells, and shows that adding AKH to PG explants stimulates calcium signalling in PG cells. In addition, silencing AKH receptor specifically in PG cells delays the larva-to-pupa transition [41]. However, whether AKH participates in the physiological response to nutrient deprivation identified here for CC-Dilps was not tested experimentally.

Storing Dilps away from general circulation

We find that preventing CC-Dilp storage increases circulating levels by 2-fold. This leads to anincrease in animal mass during the late larval stages, when circulating Dilp levels wane (compare Figures 3F and 5H ; also see Okamoto and Nishimura [42]). We also noted that such accelerated larval growth does not affect adult size due a compensatory advance in pupariation. This result suggests an interaction between the two Dilp reservoirs, where the CC-Dilp store forms from IPC-produced insulins that are rerouted from the general circulation in conditions of optimal nutrition. It has been described previously that the IPC project their termini in proximity of the CC onto the aorta. Whether CC-Dilp accumulates through local delivery of IPC-produced Dilps or by uptake from the general circulation is still unknown.

Insulins bind to their cognate receptor InR in target tissues and are then co-endocytosed and later degraded [26,43]. Our study demonstrates that the uptake of Dilps by CC cells does not rely on InR but rather Imp-L2, an alternative insulin-binding protein previously shown to bind circulating Dilps.–This result contrasts with the previously described case of Imp-L2-producing *Hugin* neurons in the larval CNS, where both InR and Imp-L2 are required for Dilp uptake [19]. This difference might have important functional consequences. In contrast to endocytosed Dilps/InR complexes, which are prone to degradation, endocytosed ImpL2/Dilp complexes are routed towards storage in DCV, in the absence of local activation

of IIS. Dilps are co-packaged with AKH in DCVs, possibly during the DCV maturation phase. This phase is characterized by cargo exchange between endo-lysosomal compartments and immature vesicles budding off from the trans-Golgi network [44]. Recent studies [28,45] suggest that RAB2 and associated proteins are involved in this exchange. However, we do not know if these components participate in routing DILPs and AKH to DCVs in the CC. Furthermore, Dilps are anterogradely transported along the axonal projections in the PG. This process is similar to the transcytosis of various trophic factors and pathogens observed in mammalian nervous systems [46]. Unlike simultaneous uptake and release previously demonstrated in other neuron types [47–49], we show here that Dilp uptake and release are temporally separated during larval development. In all, this sheds light on the unique ability of CC neurosecretory cells to convert an endocrine signal like insulin into a paracrine one.

In conclusion, we describe here a mechanism of organ sparing relying on the storage and release of insulins, allowing the maintenance of IIS activation and ecdysone production in an endocrine organ. The existence of such mechanism opens the intriguing possibility that local pools of insulin/IGF could be used in response to environmental signals to maintain IIS signalling in spared organs in other models.

Acknowledgements

This article is dedicated to the memory of our esteemed colleague and mentor Prof./Dr. Suzanne Eaton. We are grateful to Dr. Natalie Dye for her supervision and leadership. We thank Dr. Anne Grapin-Botton, Dr.Jonathan Rodenfels, the Eaton and Leopold lab members for insightful discussions and comments on the manuscript. Stocks obtained from the Bloomington Drosophila Stock Center (NIH P40OD018537) were used in this study. We would also like to thank the Prof. Linda Partridge and Dr. Jason Tennessen for providing us with fly lines, Prof. Marc Tatar and Dr. Stephanie Post for sharing reagents, and Dr. Hugo Stocker for gifting us anti-Imp-L2 antibodies. The scientific illustrations were done by Dr. Bertsy Goic. This work was supported by Deutsche Forschungsgemeinschaft (DFG/FOR2682), Max-Planck-Gesellschaft, Institut Curie and INSERM.

Author contributions

Conceptualization, S.G., S.E., P.L., Methodology, S.G., S.E., P.L., Investigation, S.G., W.L., M.W.-B., M.B.-V. Writing and editing, S.G., P.L., Funding Acquisition, S.E.; Supervision, S.G., S.E., P.L.

Declaration of interests

The authors declare no competing interests.

Figure legends

Figure 1. IPC-derived DILPs 2 and 5 accumulate in the corpora cardiaca.

(A) Neuroanatomy of the larval central nervous system and ring gland complex showing innervation of insulin-producing cells(IPC) and the corpora cardiaca(CC).

(B-C) Maximum z-volume projection of brain and ring gland complex of larvae expressing Synaptotagmin-1-GFP **(B.i and C.i, green)** specifically in the **(B)** IPC (*dilp2*-gal4) or the **(C)** CC (*akh*-gal4). Tissues are co-stained for DILP2 **(B.ii and C.ii, magenta)**. **Solid arrows** denote aortal projections from **(B)** IPC (**white arrow**) and **(D)** CC (**yellow arrow**). **Open arrows** (yellow) show CC projections to the PG. Merged channels **(B.iii and C.iii)** channel show colocalization. Scale bar = 50 µm

(D) Wild-type soma of CC cells stained for neuronal marker HRP (**D.i ; gray**), DILP2 (**D.ii, green**) and DILP5 (**D.iii, magenta**). Merged channel (**D.iv**) show DILP2 and DILP5 colocalization. **R** = pixel-based Pearson's correlation coefficient between the same. Scale bar = 10 µm.

(E,G) Soma of CC cells of IPC-specific(*dilp2*-gal4) (**E.iv-vi**)DILP2 RNAi in Dicer2-expressing background or (**G.iv-vi**) DILP5 RNAi together with wild-type controls (**E.i-iii and G.i-iii**). Stained for neuronal marker HRP(**E.i, E.iv, G.i and G.iv, gray**) and **(E)**DILP2 (**E.ii and E.v, green**) or **(G)**DILP5 (**G.ii and G.v, green**). Merged channels (E**.iii, E.vi, G.iii and G.iv**) for clarity. Scale bar = 10 µm

(F, H) Average fluorescence intensity of **(E)**DILP2 or **(G)**DILP5 normalized to the control mean. Each point represents a single soma of the CC. n =3-7; **= p<0.01, Student's t-test.

See Figure S1 and Table S1 for further information.

Figure 2. ImpL2 in the corpora cardiaca is necessary for DILP uptake.

(A) Soma of the CC specifically expressing(*akh*-gal4) Synaptotagmin-1-GFP (**A.i, yellow**); stained for nuclei (**A.i,blue**), ImpL2 (**A.ii, gray**) and DILP2 (**A.iii, green**).

(B) CC-specific(*akh*-gal4) RNAi-mediated knockdown of insulin receptor (**B.iv-vi**), ImpL2 (**B.vii-ix**) and wild-type control (**B.i-iii**). Stained for neuronal marker HRP (**B.i, B.iv, and B.vii, gray**) and DILP2 (**B.ii, B.v and B.viii, green**). Merged channels (**B.iii, B.iv and B.ix**) for clarity.

(D) CC-specific(*akh*-gal4) RNAi-mediated knockdown of ImpL2 (**d.vii-ix**) and wild-type control (**b.i-iii**). Stained for neuronal marker HRP (**b.i, b.iv, and b.vii, gray**) and AKH (**d.ii,and d.iv , blue**).

(C, E) Average fluorescence intensity of (C)DILP2 or (E)AKH normalized to the control mean. Each point represents a single soma of the CC. n =3-5; **= p<0.01, ns = p>0.01; Student's t-test.
Scale bar = 10 µm
See Figures S2, S3 and Table S1 for further information.

Figure 3. Corpora cardiaca sequesters circulating DILPs.

(A) Percentage pupariated of indicated genotype at various timepoints. Dashed line indicates 50% pupariation. Significance values represent CC>IMPL2-RNAi compared pairwise with each control. Control genotypes are not significantly different from each other (p>0.01). AEL= after egg-laying. n= 3-6 for each genotype.
(B) Pupal volume (n= 24), (C) adult weight (n=7, 9) and (D) adult wing area (n=55, 20) normalized to control. Each point represents a larva/fly in the case of pupal volume or wing area, and mean of a cohort of 8-15 flies in case of weight measurements.
(E) Larval mass of indicated genotype at specified developmental time (n=8-12). Each point represents mean of cohorts of 13-15 larvae. Significance values represent CC>IMPL2-RNAi compared pairwise with each control. Control genotypes are significantly different from each other (p<0.01).
(F) DILP2-HA-FLAG concentration in larval hemolymph of indicated genotype using driver line *akh*-gal4 containing the dilp2-HF construct (n=7,5).
(G) Fat body of indicated genotype stained for nuclei (G.i and G.iii, blue) and mCherry (G.ii and G.iv, red). White dashed outlines show the position of some nuclei in the mCherry channel. Scale bar = 50 µm.(h) Boxplots showing ratio of nuclear to cytoplasmic mCherry intensity in fat bodies. Lower ratio indicates higher insulin activity. (n= 10)
Bar plots show mean and error bars indicate standard deviation. AEL= after egg-laying. **= p<0.01, ns = p>0.01, (B-E) Student's t-test and (A,F,H) two-tailed Mann-Whitney U test.
See Table S1 for further information.

Figure 4. DILPs and AKH colocalize in corpora cardiaca dense-core vesicles.

(A) Schematic representation of experimental approach.
Electron micrograph of
(B) the soma of a CC cell (epon-embedded sections). N = nucleus, G = Golgi complex, ER = endoplasmic reticulum, and DCV= dense-core vesicle. Scale bar = 500nm.

(C) Part of cytoplasm in the soma of the CC (methylacrylate sections). DILP5 labelled with immunogold particles of 5nm diameter. Dashed red line indicates area occupied by DCVs. Scale bar = 500nm (d) Quantification of gold particle density (no. of particles/μm^2) from DCV area (dashed red line) or rest of the cytoplasm (solid black line) from multiple acquisitions (n=4). Bar plot indicates mean.

High-resolution electron micrographs of

(E) a multi-vesicular body (MVB, E.i) and a dense-core vesicle(DCV, E.ii) in soma of the CC. DILP2 and DILP5 are stained by 10nm (closed arrow) and 5nm (open arrow) immunogold particles respectively. Scale = 100nm.

(F) DCV area stained for DILP2 (10nm gold particle, closed yellow arrow) and AKH (5nm gold particle, open gray arrow). Scale bar = 100nm.

(G) Histogram showing immunogold particle size vs. frequency distribution of DILP2 (yellow) and AKH (gray)in (F) .

See Figure S4 and Table S1 for further information.

Figure 5. Corpora cardiaca DILPs enable starvation-induced accelerated pupariation.

(A) Experimental setup for larval starvation

(B-C) Means of percentage pupariation connected across timepoints for the indicated genotype- starved (dashed line) or kept feeding (solid line) as shown in (A). Fed controls are the same as shown in Figure 3a. w1118 > UAS-ImpL2-RNAi control fed and starved curves are shown in Figure S7.

n=6 for each curve; p-value from two-way ANOVA with repeated measures and Bonferroni's post t-test for multiple comparisons. Error bars indicate +/- S.D. **= $p<0.01$ and ns = $p>0.01$

(D,F) Soma of CC cells of genotype (D)*akh*>w1118 and (D)*akh*>KIR2.1 stained for HRP(D.i,D.iv, F.i and F.iv; gray) and DILP2 (D.ii, D.v, F.ii and F.v; green). KIR2.1 expression inactivates neurons. Scale bar = 10 µm.

(E,G) Average fluorescence intensity of DILP2 normalized to the mean of fed controls. Each point represents a single soma of the CC. n =3-5.

(H-I) DILP2-HA-FLAG concentration in larval hemolymph of indicated genotype using driver line *akh*-gal4,dilp2-HF (n=4-5).

(J) Fat body of indicated genotype stained for nuclei (J.i and J.iii; blue) and mCherry (J.ii and J.iv; red). White dashed outlines show the position of some nuclei in the mCherry channel. Scale bar = 50um. (K) Boxplots showing ratio of cytoplasmic to nuclear mCherry intensity in fat cells (n=5).

(L) Prothoracic gland of indicated genotype stained for nuclei (L.i, L.iii, L.v and L.vii; blue) and mCherry (L.ii, L.iv, L.vi and L.viii; red). White dashed outlines show the position of some nuclei in the mCherry channel.

Scale bar = 10 µm . **(M)** Boxplots showing ratio of nuclear to cytoplasmic mCherry intensity in prothoracic gland cells. n=4-8.

(N) Bar graph showing mean fold changes of ecdysone target genes of indicated genotype and treatment, with respect to mean of wild-type fed control (CC>w1118). Expression data normalized to housekeeping gene *rp49*. Each point represents a replicate. (n = 6)

AEL= after egg-laying. **= p<0.01, ns = p>0.01, **(E-G)** Student's t-test and **(H,I,K,M,N)** two-tailed Mann-Whitney U test.

See Figure S5 and Table S1 for further information.

STAR Methods:

Resource availability

Lead contact

Further information and requests for resources and reagents should be directed to and will be fulfilled by the Lead Contact, Pierre Leopold (pierre.leopold@curie.fr)

Material availability

This study did not generate new unique reagents.

Data and code availability

All data reported in this paper will be shared by the lead contact upon request.

This paper does not report original code. Fiji/ImageJ macros used in this study are simple (plug-in based) and/or already available in public repositories listed in the Key Resources Table.

Any additional information required to reanalyze the data reported in this paper is available from the lead contact upon request.

Experimental Model and Subject Details

All *Drosophila melanogaster* lines/crosses were maintained and grown on standard media containing cornmeal, molasses, agar and yeast extract under a 12hour light/dark cycle at 25˚C (unless explicitly stated otherwise).

Female larvae, pupae and flies were used for all size and weight measurements to prevent sex-dependent variation. In all other cases, sex was not differentiated and larvae were randomly collected. For crosses,

20-25 virgin females were crossed with 5-7 healthy males. Within 0-2 hours of hatching, not more than 30 L1 larvae were transferred to food vials to ensure absence of larval crowding.

Complete list of fly strains used in this study have been listed in the Key Resources Table. Fly strains *dilp2-Gal4,>dcr2* , *akh-Gal4,Foxo-mCherry* , *akh-Gal4,gdilp2-HF* and *ap-Gal4,tub-Gal80TS,Foxo-mCherry* were generated in this paper by crossing the listed lines.

Method Details

Developmental timing and starvation

Fly crosses were fed fresh yeast paste and allowed to lay eggs for 3 hours on apple-juice agar plates. Following egg-laying, the plates were stored at 25˚C. After 18-24 hours of incubation, freshly hatched L1 larvae were collected in PBS in intervals of 2 hours. In order to prevent overcrowding, no more than 20-30 larvae were transferred into a single food vial using a micropipette and shifted to the incubator at 25˚C with 12/12 day-night cycle. At specified time after egg-laying, larvae were carefully washed out of the food using PBS. Subsequently they were quickly transferred to 1% agar vials (same quantity as food). Fed controls were not washed out, and left to feed in their original vials. Both starved and fed control vials were returned to the same incubator.For pupariation timing, number of pupae including white pre-pupae were manually counted at fixed intervals as indicated. Counting was stopped when there was no increase for 3-4 consecutive time points. The same dataset have been used in Figure 3a, and to depict fed controls in Figure 5b,c. For all other starvation experiments, starved and fed control larvae were washed out of the 1% agar or food with PBS, rinsed and used in respective assays.

Weight measurements

To measure larval weight at specified developmental stage, larvae were collected from food/agar in PBS, washed 3x times to remove stuck food and cold-anesthetized. Female larvae were selected under the microscope to prevent sex-dependent size variation. Cohorts of 13-15 larvae were blotted on a tissue paper (to ensure no extra liquid) and transferred to a pre-weighed 1.5ml micro-centrifuge tube using forceps. The tube with larvae was then weighed using a fine balance (Sartorius). To measure adult weight, virgin females (2 days after eclosion) were anesthetized and collected in pre-weighed 1.5ml micro-centrifuge in cohorts of 10 flies per tube. The tube with adult flies was weighed using a fine balance (Sartorius). Average weight in each case was calculated by dividing the weight difference with the number of larvae/flies in each tube.

Size determination

To measure adult wing area, females (1 day after eclosion) were collected and stored in isopropanol. Prior to dissection, flies were transferred to a cavity dissection-glass. Care was taken to keep flies submerged in adequate isopropanol at all times. One wing from each fly was dissected using fine forceps (Dumont, No.5-SA) and transferred to a glass slide along with a small amount of isopropanol (in forceps due to capillary action). It is important to keep wings flat on the slide surface. This can be achieved by repeatedly moistening the wings with isopropanol, using forceps. Once the desired number of wings were obtained, 30ul of Euparal (Roth, cat#7356.1) was pipetted on the slide. Next, a glass coverslip (22mm/22mm/17µm) was placed covering the entire area on the slide occupied by wings. To ensure absence of air bubbles and minimum displacement in the wings, it is important to place the coverslip starting from one edge. Following mounting, the slides were left to dry for 2 hours prior to imaging. Single wing images were taken using Zeiss Sv11 dissection scope fitted with a CCD camera (Jenoptik ProgRes C10).

To measure pupal volume, pupae (24-30-hours APF) were collected using a wet brush. Following which, they were washed with PBS to dislodge attached food and glue. Each pupa was then transferred to a single well of a transparent 24-well plate and imaged using Zeiss Sv11 dissection scope fitted with a CCD camera (Jenoptik ProgRes C10). Sex determination was done post-eclosion and only females were taken for analysis.

Quantitative real-time PCR

Total RNA was extracted from homogenized L3 larvae using Qiagen RNeasy Mini Kit (cat #74104), from which cDNA was subsequently prepared using SuperScript III RT-PCR kit(Thermo Fisher, cat#12574026). Purity of RNA and DNA were checked by measuring absorbance using a NanoDrop 2000 (Thermo Fisher scientific). qRT-PCR was performed using SYBR green (Roche FastStart Essential, cat#06402712001) on a Roche LightCycler 96 instrument. Data analysis was done using LightCycler 4.1 software (Roche). Standard curves were generated for each primer pair. Primers were adapted from a recent publication[50]. All expression levels were normalized to the housekeeping gene *rp49*. The fold changes in expression were calculated using relative quantification function. Expression values are representated as fold changes as compared to the control.

Dilp2-HF ELISA

Nunc MaxiSorp Flat-Bottom plates (Thermo Fisher Scientific) were coated with anti-FLAG M2 antibody (Sigma, cat#F1804) diluted in BupH Carbonate-Bicarbonate Buffer (Thermo Fisher Scientific, cat#28382) overnight at 4˚C. The plates were washed 2x in wash buffer – PBS + 0.2% Tween20 (Sigma, cat#P7949) and blocked in 2% filter-sterilized BSA in PBS overnight at 4˚C. 1µL of hemolymph was collected by bleeding 5-8 heterozygous gDilp2-HF larvae on a clean cavity slide. The hemolymph was diluted in 55mL PBS and centrifuged at 10,000rpm for 10 minutes to remove hemocytes and debris. 50mL supernatant and 1mL of anti-HA-HRP antibody (Roche, cat#12013819001) solution (1:500) was incubated in the coated wells overnight at 4˚C. 100 ml of 1-Step-Ultra TMB-ELISA Substrate (Thermo Fisher, cat#34028) was pipetted to each well and incubated for 30 minutes in dark at room temperature. Reaction was stopped by adding 100 ml of 2M sulfuric acid per well. The samples colorized instantly and the absorbance was measured immediately at 450nm using a plate reader (BMG Labtech). Standard curve was generated by self-generated FLAG(GS)HA peptide. The detailed method is described here [51].

Immunofluorescence

Freshly dissected tissue in PBS was fixed with 4% paraformaldehyde (cat#16005, Aldrich) for 20 minutes. After fixation, tissues were thoroughly washed 3-4 times with PBS. The following protocol was used depending on tissue type. For brain, ring gland and fat body, tissues were permeabilized with PBS containing 0.2%(v/v) Triton X-100(Serva Electrophoresis GmbH, cat#37240.01) for 2 hours at room temperature with shaking. Primary incubation with antibody was done overnight in incubation buffer- PBS with 0.2% Triton X-100 (PBST) and 1mg/ml bovine serum albumin (BSA) (Sigma, cat#A2153). Incubation was followed by 3x15 minute washes with the same incubation buffer without antibodies. Secondary incubation was done with antibody diluted in incubation buffer supplemented with 4%(v/v) normal goat serum (NGS) overnight at 4˚C. Tissues were then washed 4X15 minutes in 0.2%PBST and mounted on glass slides using VectaShield H-1000(cat# H-1000-10) mounting medium. Wing discs were permeabilized with PBS containing 0.05%(v/v) Triton X-100 supplemented with 1mg/ml bovine serum albumin (BSA) and 250mM NaCl for 3X10 minutes at room temperature with shaking. Primary incubation with antibody was done overnight in incubation buffer- PBS with 0.05% Triton X-100 (PBST) and 1mg/ml bovine serum albumin (BSA). Incubation was followed by 3x15 minute washes with the same incubation buffer without antibodies. Secondary incubation was done with antibody diluted in incubation buffer supplemented with 4%(v/v) normal goat serum (NGS) for 2-3 hours. Wing discs were then washed 3X15 minutes in 0.1%PBST and mounted on glass slides using VectaShield H-1000 mounting medium. All washing and incubation

steps were performed on a shaker. Fat bodies from late larval stages disintegrate easily and requires extra care while handling, preferably shaking at a low rpm.

Confocal laser scanning microscopy

Three imaging setups were used in this paper. First, Olympus FV1000 laser scanning confocal microscope on Olympus BX61 inverted stand and driven by FV10-ASW 1.7 software. Brain and ring gland whole mounts were imaged with Olympus UApochromat 40x 1.3NA oil immersion objective. Corpora cardiaca cells were imaged with Olympus UApochromat 60x 1.35 NA oil immersion objective. Second, Andor spinning disc confocal microscope on Olympus IX81 inverted stand using Andor iXON 897 EMCCD camera with Yokogawa CSUX1 scanhead, running on Andor software. Some fat bodies were imaged with Olympus U Plan SApo 60x/ 1.35NA oil immersion objective. Third, Olympus FV3000 laser scanning confocal microscope on Olympus IX83 inverted stand and driven by FV31S-SW acquisition software. Corpora cardiaca cells and wing discs were imaged with Olympus UPLXApochromat 60x 1.42 NA oil immersion objective.

Electron microscopy

Morphology: Dissected brain-ring gland complexes were initially fixed in PBS with 2%PFA (cat#16005, Aldrich) and 1% glutaraldehyde (cat#G5882, Sigma) for 2 hours at room temperature followed by overnight incubation at 4˚C. Then the samples were post-fixed with 1% OsO4 (cat# 19190, EMS) and 1.5% potassium ferrocyanide (cat#: P9387, Sigma-Aldrich) in water on ice for 1 hour. En bloc staining was done in the dark with 1% UA (cat# 21447, Polyscience Europe GmbH) in water at 4˚C overnight. Following infiltration and embedding, 70nm sections were cut on a Leica Ultracut UCT (Leica Microscopy systems) and picked up with formvar (cat# 15800, EMS) coated slot grids (cat# G2010-Cu, EMS). All samples were then post-stained with 1% UA (cat# 21447, Polysciences Europe GmbH) in water for 10 minutes and 0.04% lead citrate (cat# 17800, EMS) for 5 minutes. Electron micrographs were obtained at 80kV using Morgagni (Emsis Morada CCD camera, formerly Sys/Olympus) and 100kV using Tecnai 12 (TVIPS F416 camera) electron microscopes (both from Thermo Fisher Scientific (formerly FEI/Philips)). **Immunogold labelling:** Dissected brain-ring gland complexes were initially fixed in PBS with 4% PFA and 0.05% glutaraldehyde for 20 minutes at room temperature. Post-fixation was done in 1:1 dilution of the initial fixative overnight at 4˚C. Ring glands were then embedded with 12% gelatin (cat# G-2500, Sigma-Aldrich) in PBS and infiltrated with 2.3M sucrose (cat# 21600, EMS) in PBS overnight at 4˚C. The sucrose infiltrated Ring gland in gelatin was mounted on an aluminum pin and snap frozen in liquid nitrogen and cryosectioned on a Leica Ultracut EM UC6 ultramicrotome (Leica Microscopy systems). 70nm Sections

were picked up using a 1 :1 mixture of 2.3M sucrose and 2% methyl cellulose (cat# M-6385, Sigma-Aldrich) as a pick-up solution and sections were transferred to carbon and formvar coated mesh grids (cat# H100-Cu, EMS). After removal of gelatin by incubation on PBS at 37 ˚C, sections were labelled with rabbit-anti-Dilp2/Dilp5 or goat-anti-AKH Antibody (diluted 1 to 20 or 1 to 100 from original antibody solution) followed by secondary antibody coupled to 10-nm gold (British Biocell or Bbisolutions) and secondary fluorescence antibodies (donkey-anti-rat AlexaFluor-594 cat# A-21209, Molecular Probes Europe B.V., goat-anti-rabbit AlexaFluor- 488 cat# A-21206, Mol. Probes Europe B.V.) The sections were first imaged with epifluorescence on a Zeiss upright ApoTome microscope with Axiocam506 camera to locate regions of interest in individual sections (Figure S4) and contrasted with a mixture of 1.9% methyl cellulose/0.3% UA for 10min on ice and the corresponding regions of interest were observed by using a Morgagni or Tecnai12 electron microscope.

Quantification and Statistical Analysis

Whole cell: Individual cells from multiple samples were manually segmented and mean intensity was measured using Fiji/ImageJ [52] .**Co-localization :** Single confocal images from two different channels were used in Coloc 2 plugin in Fiji/ImageJ. **Nuclear and cytoplasmic intensity ratio:** Regions of interest were manually drawn on respective tissues. Nuclear to cytoplasmic intensity ratio was then calculated using a Fiji/ImageJ macro developed by Volker Baecker at Montpellier RIO Imaging (Intensity Ratio Nuclei Cytoplasm Tool, RRID:SCR_018673). Documentation can be accessed here . Same analysis parameters were used across samples compared. **Electron micrographs:** For morphological sections, composite images were assembled in Fiji [52] using ImageJ TrackEM2 plugin [53]. For immunogold labelling, regions of interest were visually determined and gold particles were hand-counted in Fiji/ImageJ. **Wing area:** Each wing blade was hand segmented and area measured in pixels using a self-written macro on Fiji/ImageJ. **Pupal volume:** Using a self-written Fiji/Imagej macro, an ellipse was fitted to the pupa. Volume was calculated assuming an ellipsoid using the formula below (minor axis length as the height) -

Volume = 0.75π*(major-axis) * $(\text{minor-axis})^2$.

Data wrangling was done using Microsoft Excel and R-Studio (version 1.3.1093). R-Studio was also used for plotting. Packages used in R- plyr, dplyr, ggplot2 and xlsx. Plots generated through R were then formatted using Adobe Illustrator 2021. Illustrations were generated using BioRender (www.biorender.com). Statistical analysis was done using Microsoft Excel, GraphPad Prism 5.0 and online through https://www.socscistatistics.com . Information about sample sizes and statistical tests used in this study can be found in the respective figure legends. Detailed information on sample size and replicates have also been summarized in **Table S1** of the supplementary material.

References

1. Petersen MC, Shulman GI. Mechanisms of insulin action and insulin resistance. *Physiol Rev*. 2018;98(4):2133-2223. doi:10.1152/physrev.00063.2017
2. Campbell JE, Newgard CB. Mechanisms controlling pancreatic islet cell function in insulin secretion. *Nat Rev Mol Cell Biol*. 2021;22(2):142-158. doi:10.1038/s41580-020-00317-7
3. Tokarz VL, MacDonald PE, Klip A. The cell biology of systemic insulin function. *J Cell Biol*. 2018;217(7):2273-2289. doi:10.1083/jcb.201802095
4. Wang Y, Bikle DD, Chang W. Autocrine and Paracrine Actions of IGF-I Signaling in Skeletal Development. *Bone Res*. 2013;1:249-259. doi:10.4248/BR201303003
5. Fernandez AM, Torres-Alemán I. The many faces of insulin-like peptide signalling in the brain. *Nat Rev Neurosci*. 2012;13(4):225-239. doi:10.1038/nrn3209
6. Popken GJ, Hodge RD, Ye P, et al. In vivo effects of insulin-like growth factor-I (IGF-I) on prenatal and early postnatal development of the central nervous system. *Eur J Neurosci*. 2004;19(8):2056-2068. doi:10.1111/j.0953-816X.2004.03320.x
7. D'Ercole AJ, Ye P. Minireview: Expanding the mind: Insulin-like growth factor I and brain development. *Endocrinology*. 2008;149(12):5958-5962. doi:10.1210/en.2008-0920
8. Spéder P, Brand AH. Systemic and local cues drive neural stem cell niche remodelling during neurogenesis in drosophila. *Elife*. 2018;7:1-16. doi:10.7554/eLife.30413
9. Id XY, Id CWS, Suzawa M, Id MLB, Id ES. Dilp-2 – mediated PI3-kinase activation coordinates reactivation of quiescent neuroblasts with growth of their glial stem cell niche. 2020:1-23. doi:10.1371/journal.pbio.3000721
10. Cox P, Marton T. Pathological assessment of intrauterine growth restriction. *Best Pract Res Clin Obstet Gynaecol*. 2009;23(6):751-764. doi:10.1016/j.bpobgyn.2009.06.006
11. Cheng LY, Bailey AP, Leevers SJ, Ragan TJ, Driscoll PC, Gould AP. Anaplastic Lymphoma Kinase Spares Organ Growth during Nutrient Restriction in Drosophila. *Cell*. 2011;146(3):435-447. doi:10.1016/j.cell.2011.06.040
12. Kim SK, Rulifson EJ. Conserved mechanisms of glucose sensing and regulation by Drosophila corpora cardiaca cells. 2004;431(September):316-320. doi:10.1038/nature02913.1.
13. Rulifson EJ. Ablation of Insulin-Producing Neurons in Flies: Growth and Diabetic Phenotypes. *Science (80-)*. 2002;296(5570):1118-1120. doi:10.1126/science.1070058
14. Jan LY, Jan YN. Antibodies to horseradish peroxidase as specific neuronal markers in Drosophila and in grasshopper embryos. *Proc Natl Acad Sci U S A*. 1982;79(8):2700-2704. doi:10.1073/pnas.79.8.2700

15. Honegger B, Galic M, Köhler K, et al. Imp-L2, a putative homolog of vertebrate IGF-binding protein 7, counteracts insulin signaling in Drosophila and is essential for starvation resistance. *J Biol*. 2008;7(3). doi:10.1186/jbiol72
16. Figueroa-Clarevega A, Bilder D. Malignant drosophila tumors interrupt insulin signaling to induce cachexia-like wasting. *Dev Cell*. 2015;33(1):47-56. doi:10.1016/j.devcel.2015.03.001
17. Lee GJ, Han G, Yun HM, et al. Steroid signaling mediates nutritional regulation of juvenile body growth via IGF-binding protein in Drosophila. *Proc Natl Acad Sci U S A*. 2018;115(23):5992-5997. doi:10.1073/pnas.1718834115
18. Roed NK, Viola CM, Kristensen O, et al. Structures of insect Imp-L2 suggest an alternative strategy for regulating the bioavailability of insulin-like hormones. *Nat Commun*. 2018;9(1). doi:10.1038/s41467-018-06192-3
19. Bader R, Sarraf-Zadeh L, Peters M, et al. The IGFBP7 homolog Imp-L2 promotes insulin signaling in distinct neurons of the Drosophila brain. *J Cell Sci*. 2013;126(12):2571-2576. doi:10.1242/jcs.120261
20. Siegmund T, Korge G. Innervation of the ring gland of drosophila melanogaster. *J Comp Neurol*. 2001;431(4):481-491. doi:10.1002/1096-9861(20010319)431:4<481::AID-CNE1084>3.0.CO;2-7
21. Grönke S, Clarke D-F, Broughton SJ, Andrews TD, Partridge L. Molecular Evolution and Functional Characterization of Drosophila Insulin-Like Peptides. *PLoS Genet*. 2010;6(2):18. doi:10.1371/journal.pgen.1000857
22. Brogiolo W, Stocker H, Ikeya T, Rintelen F, Fernandez R, Hafen E. An evolutionarily conserved function of the drosophila insulin receptor and insulin-like peptides in growth control. *Curr Biol*. 2001;11(4):213-221. doi:10.1016/S0960-9822(01)00068-9
23. Ikeya T, Galic M, Belawat P, Nairz K, Hafen E, Zu C-. Nutrient-Dependent Expression of Insulin-like Peptides from Neuroendocrine Cells in the CNS Contributes to Growth Regulation in Drosophila. 2002;12(02):1293-1300.
24. Géminard C, Rulifson EJ, Léopold P. Remote Control of Insulin Secretion by Fat Cells in Drosophila. *Cell Metab*. 2009;10(3):199-207. doi:10.1016/j.cmet.2009.08.002
25. Willey RB, Chapman GB. The ultrastructure of certain components of the corpora cardiaca in orthopteroid insects. *J Ultrasructure Res*. 1960;4(1):1-14. doi:10.1016/S0022-5320(60)80002-0
26. Sorkin A, Von Zastrow M. Endocytosis and signalling: Intertwining molecular networks. *Nat Rev Mol Cell Biol*. 2009;10(9):609-622. doi:10.1038/nrm2748
27. Cosker KE, Segal RA. Neuronal signaling through endocytosis. *Cold Spring Harb Perspect Biol*. 2014;6(2). doi:10.1101/cshperspect.a020669

650 28. Gondré-Lewis MC, Park JJ, Loh YP. *Cellular Mechanisms for the Biogenesis and Transport of*
651 *Synaptic and Dense-Core Vesicles*. Vol 299. Elsevier; 2012. doi:10.1016/B978-0-12-394310-
652 1.00002-3
653 29. Edgar BA. How flies get their size: Genetics meets physiology. *Nat Rev Genet*. 2006;7(12):907-916.
654 doi:10.1038/nrg1989
655 30. Pan X, Neufeld TP, Connor MBO, Pan X, Neufeld TP, Connor MBO. A Tissue- and Temporal-Specific
656 Autophagic Switch A Tissue- and Temporal-Specific Autophagic Switch Controls Drosophila Pre-
657 metamorphic Nutritional Checkpoints. *Curr Biol*. 2019:1-12. doi:10.1016/j.cub.2019.07.027
658 31. Tatum EL, Clancy CW. Biological Bulletin,. 75(3):447-462.
659 32. Xie X-J, Hsu F-N, Gao X, et al. CDK8-Cyclin C Mediates Nutritional Regulation of Developmental
660 Transitions through the Ecdysone Receptor in Drosophila. *PLoS Biol*. 2015;13(7):1002207.
661 doi:10.1371/journal.pbio.1002207
662 33. Kim J, Neufeld TP. Dietary sugar promotes systemic TOR activation in Drosophila through AKH-
663 dependent selective secretion of Dilp3. *Nat Commun*. 2015;6:6846. doi:10.1038/ncomms7846
664 34. Colombani J. Antagonistic Actions of Ecdysone and Insulins Determine Final Size in Drosophila.
665 *Science (80-)*. 2005;310(5748):667-670. doi:10.1126/science.1119432
666 35. Boulan L, Martín D, Milán M. Bantam miRNA promotes systemic growth by connecting insulin
667 signaling and ecdysone production. *Curr Biol*. 2013;23(6):473-478. doi:10.1016/j.cub.2013.01.072
668 36. Karim FD, Guild GM, Thummel CS. The Drosophila Broad-Complex plays a key role in controlling
669 ecdysoneregulated gene expression at the onset of metamorphosis. *Development*.
670 1993;118(3):977-988. doi:10.1242/dev.118.3.977
671 37. King-Jones K, Charles JP, Lam G, Thummel CS. The ecdysone-induced DHR4 orphan nuclear
672 receptor coordinates growth and maturation in Drosophila. *Cell*. 2005;121(5):773-784.
673 doi:10.1016/j.cell.2005.03.030
674 38. Karim FD, Thummel CS. Ecdysone coordinates the timing and amounts of E74A and E74B
675 transcription in Drosophila. *Genes Dev*. 1991;5(6):1067-1079. doi:10.1101/gad.5.6.1067
676 39. Pan X, Neufeld TP, O'Connor MB. A Tissue- and Temporal-Specific Autophagic Switch Controls
677 Drosophila Pre-metamorphic Nutritional Checkpoints. *Curr Biol*. 2019;29(17):2840-2851.e4.
678 doi:10.1016/j.cub.2019.07.027
679 40. Pan X, O'Connor MB. Coordination among multiple receptor tyrosine kinase signals controls
680 drosophila developmental timing and body size. *bioRxiv*. 2020:1-43.
681 doi:10.1101/2020.09.01.278382
682 41. Hughson BN, Shimell MJ, O'Connor MB. AKH Signaling in D. melanogaster Alters Larval

Development in a Nutrient-Dependent Manner That Influences Adult Metabolism. *Front Physiol*. 2021;12(February):1-15. doi:10.3389/fphys.2021.619219

42. Okamoto N, Nishimura T. Signaling from Glia and Cholinergic Neurons Controls Nutrient-Dependent Production of an Insulin-like Peptide for Drosophila Body Growth. *Dev Cell*. 2015;35(3):295-310. doi:10.1016/j.devcel.2015.10.003

43. Sopko R, Perrimon N. Receptor tyrosine kinases in Drosophila development. *Cold Spring Harb Perspect Biol*. 2013;5(6):1-31. doi:10.1101/cshperspect.a009050

44. Topalidou I, Cattin-Ortolá J, Pappas AL, et al. The EARP Complex and Its Interactor EIPR-1 Are Required for Cargo Sorting to Dense-Core Vesicles. *PLoS Genet*. 2016;12(5):1-29. doi:10.1371/journal.pgen.1006074

45. Lund VK, Lycas MD, Schack A, Andersen RC, Gether U. Rab2 drives axonal transport of dense core vesicles and lysosomal organelles. 2020:1-52.

46. Von Bartheld CS. Axonal Transport and Neuronal Transcytosis of Trophic Factors, Tracers, and Pathogens. *J Neurobiol*. 2004;58(2):295-314. doi:10.1002/neu.10315

47. Von Bartheld CS, Wang XX, Butowt R. Anterograde axonal transport, transcytosis, and recycling of neurotrophic factors: The concept of trophic currencies in neural networks. *Mol Neurobiol*. 2001;24(1-3):1-28. doi:10.1385/MN:24:1-3:001

48. Yamashita N, Joshi R, Zhang S, Zhang ZY, Kuruvilla R. Phospho-Regulation of Soma-to-Axon Transcytosis of Neurotrophin Receptors. *Dev Cell*. 2017;42(6):626-639.e5. doi:10.1016/j.devcel.2017.08.009

49. Hémar A, Olivo JC, Williamson E, Saffrich R, Dotti CG. Dendroaxonal transcytosis of transferrin in cultured hippocampal and sympathetic neurons. *J Neurosci*. 1997;17(23):9026-9034. doi:10.1523/jneurosci.17-23-09026.1997

50. Santabárbara-Ruiz P, Léopold P. An Oatp transporter-mediated steroid sink promotes tumor-induced cachexia in Drosophila. *Dev Cell*. 2021;56(19):2741-2751.e7. doi:10.1016/j.devcel.2021.09.009

51. Park S, Alfa RW, Topper SM, Kim GES, Kockel L, Kim SK. A Genetic Strategy to Measure Circulating Drosophila Insulin Reveals Genes Regulating Insulin Production and Secretion. *PLoS Genet*. 2014;10(8). doi:10.1371/journal.pgen.1004555

52. Schindelin J, Arganda-Carreras I, Frise E, et al. Fiji: An open-source platform for biological-image analysis. *Nat Methods*. 2012;9(7):676-682. doi:10.1038/nmeth.2019

53. Cardona A, Saalfeld S, Schindelin J, et al. TrakEM2 software for neural circuit reconstruction. *PLoS One*. 2012;7(6). doi:10.1371/journal.pone.0038011

54. Isabel G, Martin JR, Chidami S, Veenstra JA, Rosay P. AKH-producing neuroendocrine cell ablation decreases trehalose and induces behavioral changes in Drosophila. *Am J Physiol - Regul Integr Comp Physiol*. 2005;288(2 57-2):531-538. doi:10.1152/ajpregu.00158.2004

55. Tennessen JM, Baker KD, Lam G, Evans J, Thummel CS. The Drosophila estrogen-related receptor directs a metabolic switch that supports developmental growth. *Cell Metab*. 2011;13(2):139-148. doi:10.1016/j.cmet.2011.01.005

56. Kakanj P, Moussian B, Grönke S, et al. Insulin and TOR signal in parallel through FOXO and S6K to promote epithelial wound healing. *Nat Commun*. 2016;7:12972. doi:10.1038/ncomms12972

57. Khaliullina H, Panáková D, Eugster C, et al. Patched regulates Smoothened trafficking using lipoprotein-derived lipids Patched regulates Smoothened trafficking using lipoprotein-derived lipids. 2009;4121:4111-4121. doi:10.1242/dev.041392

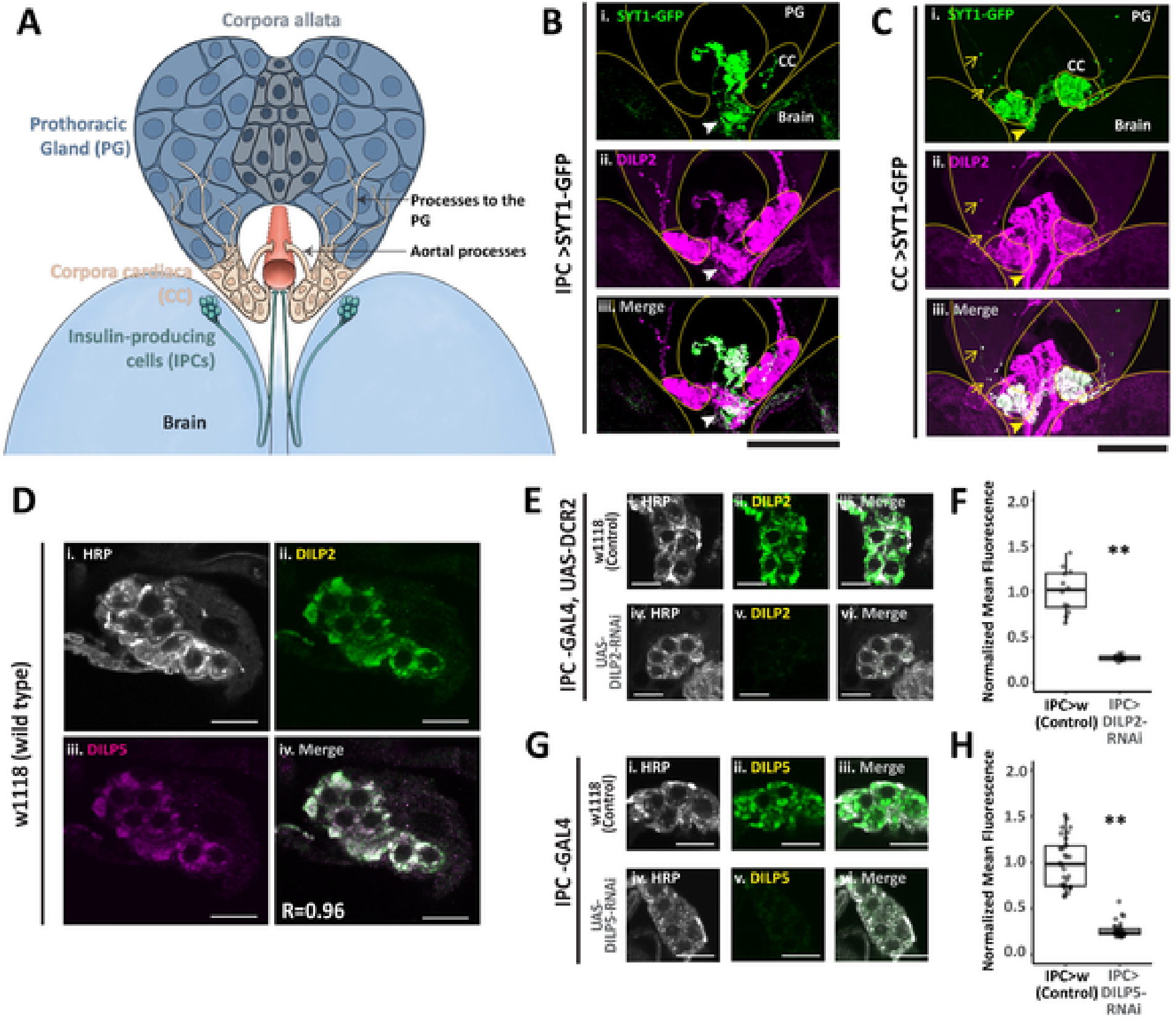
A
Corpora allata
Prothoracic Gland (PG)
Processes to the PG
Aortal processes
Corpora cardiaca (CC)
Insulin-producing cells (IPCs)
Brain
B
IPC >SYT1-GFP
i. SYT1-GFP
PG
CC
Brain
ii. DILP2
iii. Merge
C
CC >SYT1-GFP
i. SYT1-GFP
PG
CC
Brain
ii. DILP2
iii. Merge
D
w1118 (wild type)
i. HRP
ii. DILP2
iii. DILP5
iv. Merge
R=0.96
E
IPC -GAL4, UAS-DCR2
w1118 (Control)
i. HRP
ii. DILP2
iii. Merge
UAS-DILP2-RNAi
iv. HRP
v. DILP2
vi. Merge
F
Normalized Mean Fluorescence
2.0
1.5
1.0
0.5
0.0
**
IPC>w (Control)
IPC> DILP2-RNAi
G
IPC -GAL4
w1118 (Control)
i. HRP
ii. DILP5
iii. Merge
UAS-DILP5-RNAi
iv. HRP
v. DILP5
vi. Merge
H
Normalized Mean Fluorescence
2.0
1.5
1.0
0.5
0.0
**
IPC>w (Control)
IPC> DILP5-RNAi

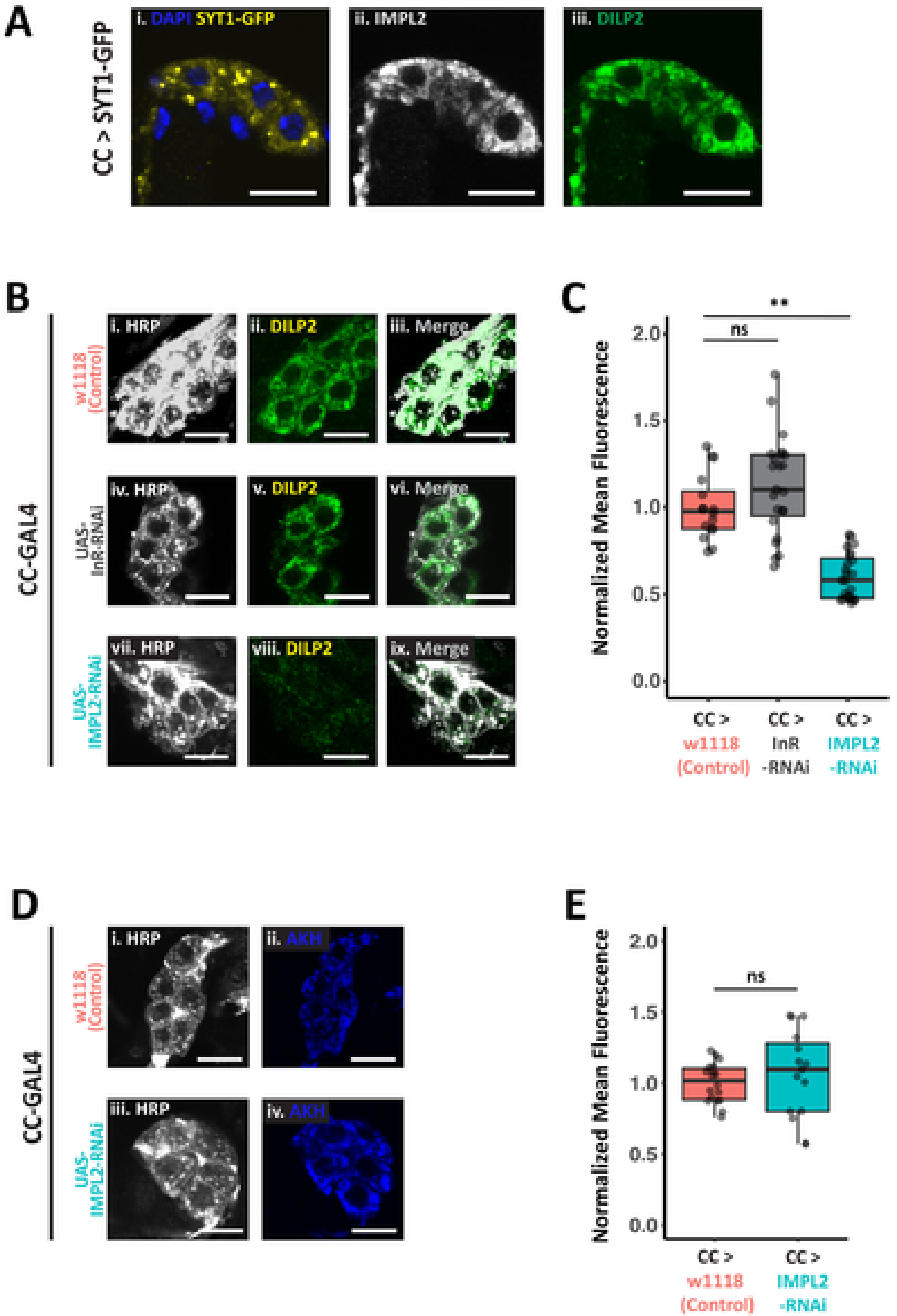
A
CC > SYT1-GFP
i. DAPI SYT1-GFP
ii. IMPL2
iii. DILP2
B
CC-GAL4
w1118 (Control)
UAS-InR-RNAi
UAS-IMPL2-RNAi
i. HRP
ii. DILP2
iii. Merge
iv. HRP
v. DILP2
vi. Merge
vii. HRP
viii. DILP2
ix. Merge
C
Normalized Mean Fluorescence
ns
**
2.0
1.5
1.0
0.5
0.0
CC > w1118 (Control)
CC > InR -RNAi
CC > IMPL2 -RNAi
D
CC-GAL4
w1118 (Control)
UAS-IMPL2-RNAi
i. HRP
ii. AKH
iii. HRP
iv. AKH
E
Normalized Mean Fluorescence
ns
2.0
1.5
1.0
0.5
0.0
CC > w1118 (Control)
CC > IMPL2 -RNAi

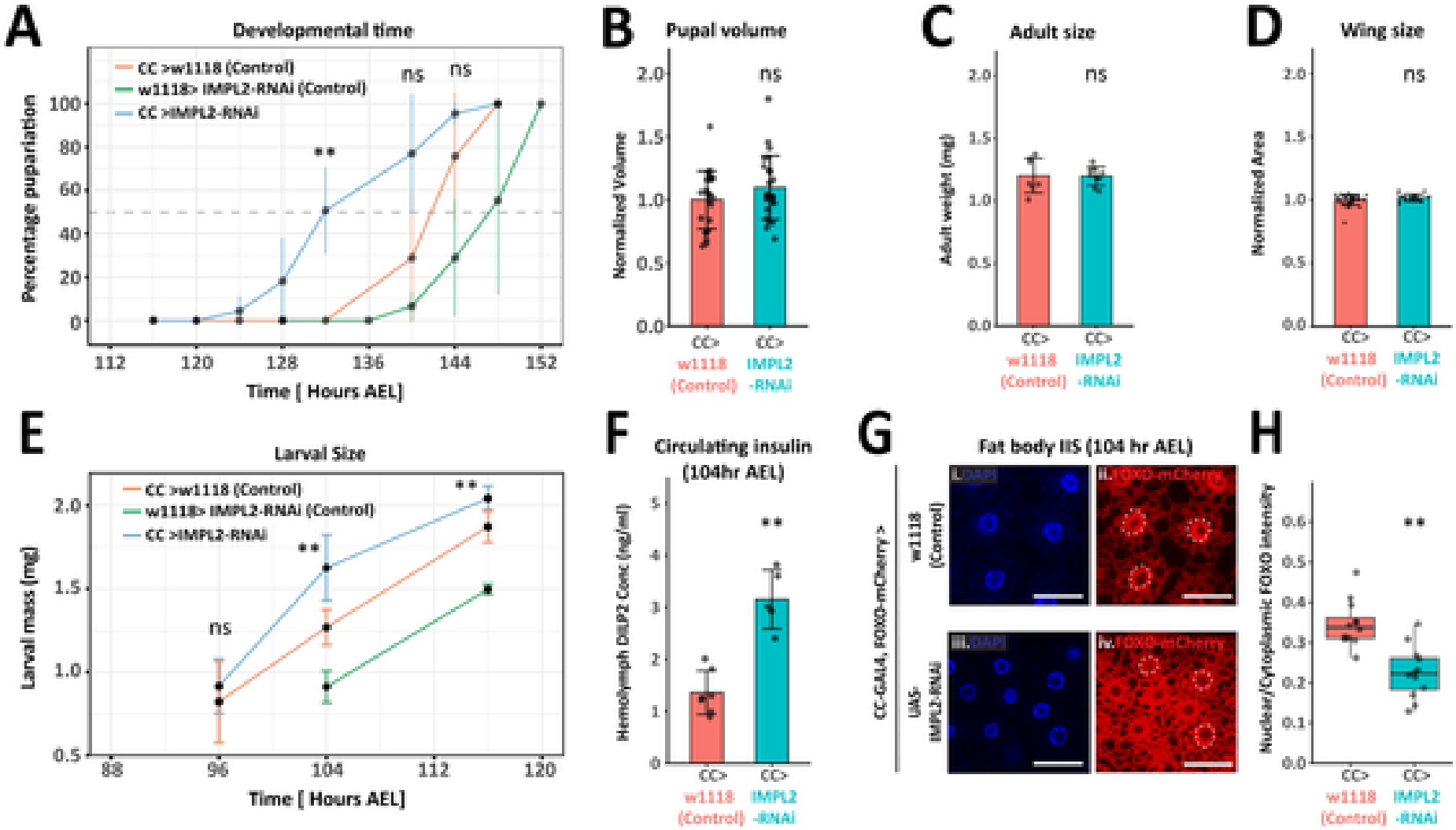
A
Developmental time
CC >w1118 (Control)
w1118> IMPL2-RNAi (Control)
CC >IMPL2-RNAi
Percentage pupariation
Time [Hours AEL]
ns
ns
**
B
Pupal volume
Normalised Volume
ns
CC> w1118 (Control)
CC> IMPL2 -RNAi
C
Adult size
Adult weight (mg)
ns
D
Wing size
Normalised Area
ns
E
Larval Size
CC >w1118 (Control)
w1118> IMPL2-RNAi (Control)
CC >IMPL2-RNAi
Larval mass (mg)
Time [Hours AEL]
ns
**
**
F
Circulating insulin (104hr AEL)
Hemolymph DILP2 Conc (ng/ml)
**
G
Fat body IIS (104 hr AEL)
CC-GAL4, FOXO-mCherry >
w1118 (Control)
UAS-IMPL2-RNAi
i. DAPI
ii. FOXO-mCherry
iii. DAPI
iv. FOXO-mCherry
H
Nuclear/Cytoplasmic FOXO intensity
**

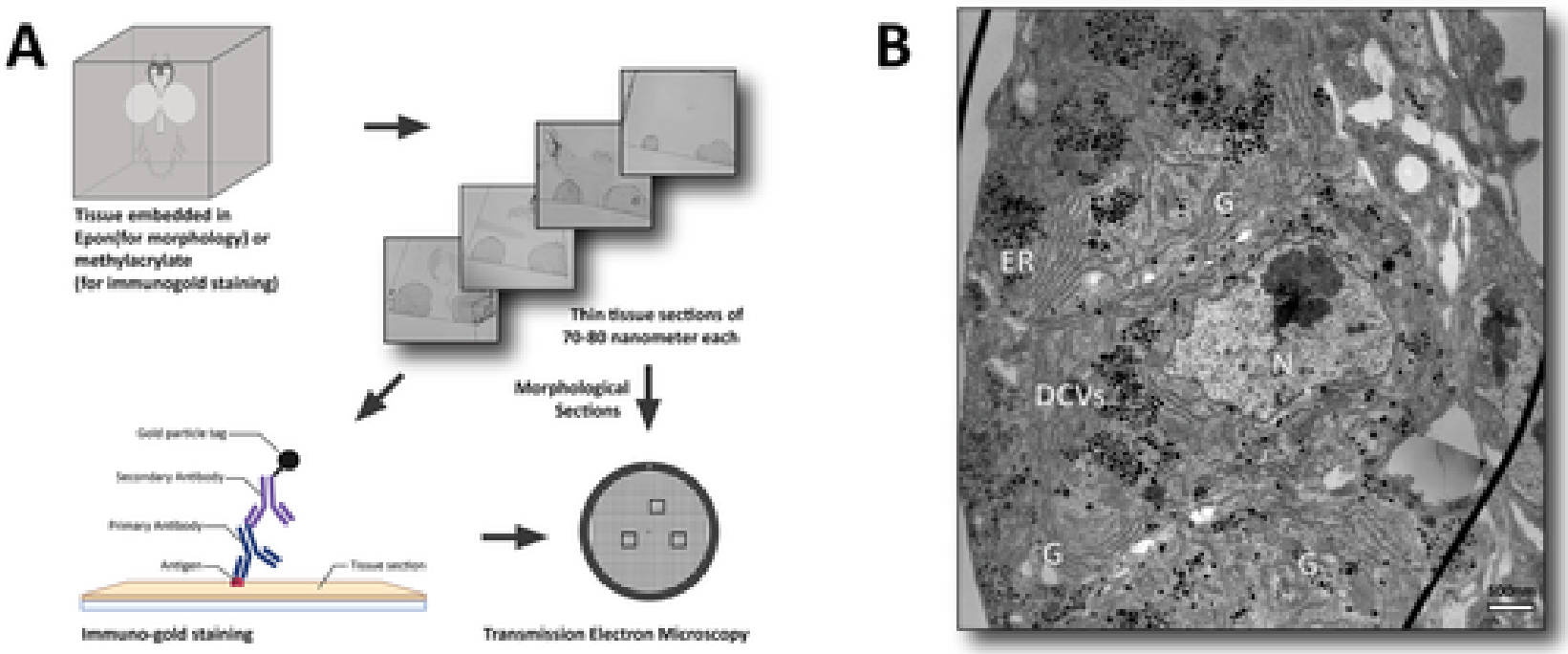
A
Tissue embedded in Epon(for morphology) or methylacrylate (for immunogold staining)
Thin tissue sections of 70-80 nanometer each
Morphological Sections
Gold particle tag
Secondary Antibody
Primary Antibody
Antigen
Tissue section
Immuno-gold staining
Transmission Electron Microscopy
B
ER
G
N
DCVs
G
G
C
DILP5 - 5nm particles
100nm
Dense-core vesicle area
D
Particle density (#particles/um)
50
40
30
20
10
0
Outside DCVs
Inside DCVs
E
DILP2 (10nm)
DILP5 (5nm)
i. MVB
100nm
ii. DCV
100nm
F
DILP2 (10nm)
AKH (5nm)
100nm
G
Particle size distribution
DILP2 (10nm)
AKH (5nm)
Number of particles
40
30
20
10
0
0
2.5
5.0
7.5
10.0
12.5
Size(nm)

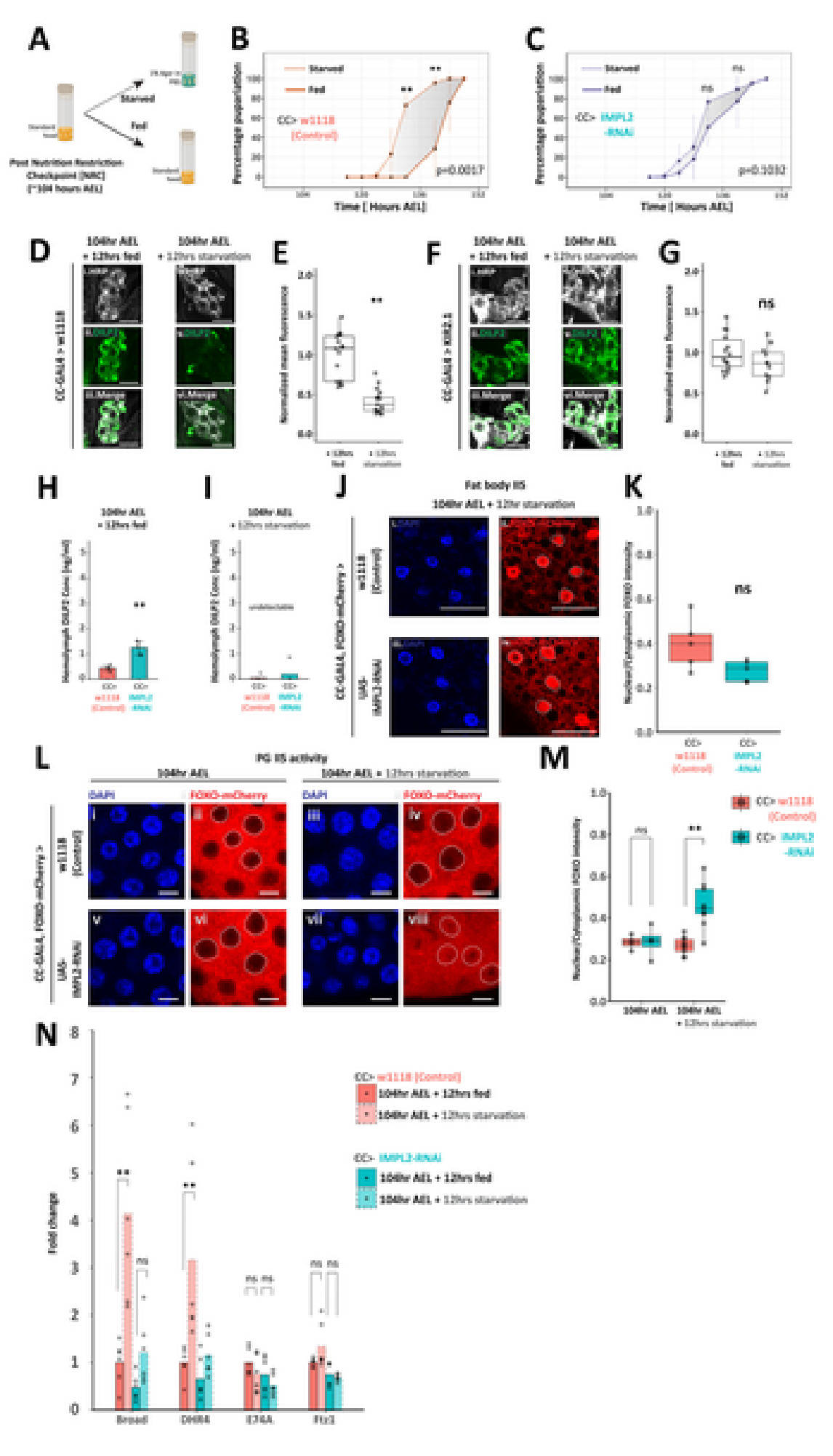
A
Starved
Fed
Post Nutrition Restriction Checkpoint [NRC] (~104 hours AEL)
B
Starved
fed
CC> w1118 (Control)
p=0.0017
Time [Hours AEL]
C
Starved
fed
CC> IMPL2 -RNAi
ns
p=0.1032
Time [Hours AEL]
D
104hr AEL + 12hrs fed
104hr AEL + 12hrs starvation
CC-GAL4 > w1118
DAPI
IMPL2
Merge
E
Normalized mean fluorescence
+ 12hrs fed
+ 12hrs starvation
F
104hr AEL + 12hrs fed
104hr AEL + 12hrs starvation
CC-GAL4 > IMPL2
G
Normalized mean fluorescence
ns
+ 12hrs fed
+ 12hrs starvation
H
104hr AEL + 12hrs fed
Hemolymph ILP1 Conc (ng/ml)
CC> w1118 (Control)
CC> IMPL2 -RNAi
I
104hr AEL + 12hrs starvation
Hemolymph ILP1 Conc (ng/ml)
CC> w1118 (Control)
CC> IMPL2 -RNAi
J
Fat body IIS
104hr AEL + 12hr starvation
CC-GAL4, FOXO-mCherry >
w1118 (Control)
UAS-IMPL2-RNAi
DAPI
K
Nuclear/Cytoplasmic FOXO intensity
ns
CC> w1118 (Control)
CC> IMPL2 -RNAi
L
FG IIS activity
104hr AEL
104hr AEL + 12hrs starvation
DAPI
FOXO-mCherry
CC-GAL4, FOXO-mCherry >
w1118 (Control)
UAS-IMPL2-RNAi
i
ii
iii
iv
v
vi
vii
viii
M
Nuclear/Cytoplasmic FOXO intensity
ns
**
CC> w1118 (Control)
CC> IMPL2 -RNAi
104hr AEL
104hr AEL + 12hrs starvation
N
fold change
CC> w1118 (Control)
104hr AEL + 12hrs fed
104hr AEL + 12hrs starvation
CC> IMPL2-RNAi
104hr AEL + 12hrs fed
104hr AEL + 12hrs starvation
Broad
D46A
E74A
Ftz1

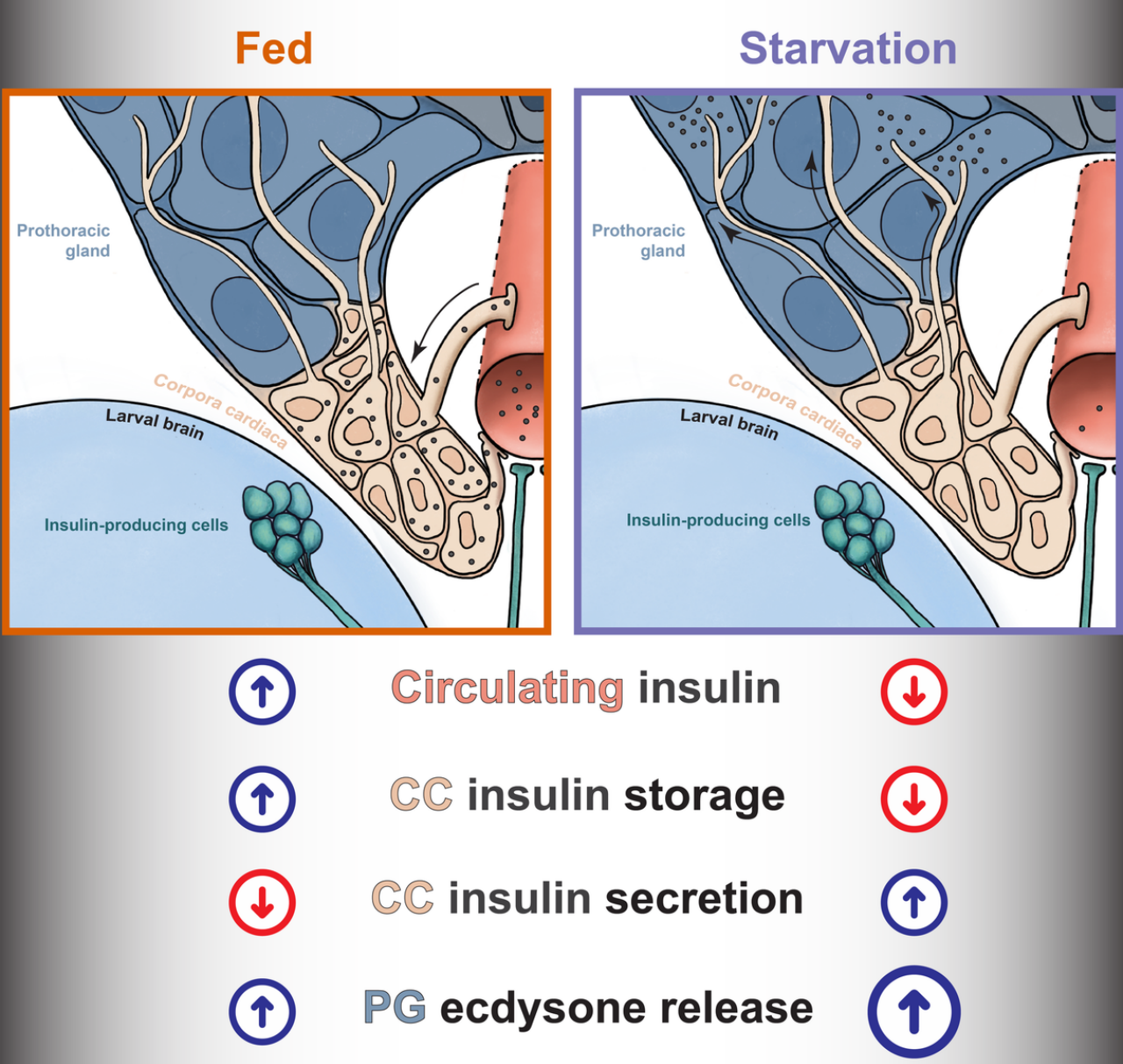
Fed
Starvation
Prothoracic gland
Corpora cardiaca
Larval brain
Insulin-producing cells
Prothoracic gland
Corpora cardiaca
Larval brain
Insulin-producing cells
Circulating insulin
CC insulin storage
CC insulin secretion
PG ecdysone release